Titanium valorization: From chemical milling baths to air depollution applications

Julie Hot, Ariane Dasque, Jivko Topalov, Vanessa Mazars, Erick Ringot

Titanium valorization: From chemical milling baths to air depollution applications

Julie Hot [a, *], Ariane Dasque [a, 1], Jivko Topalov [a], Vanessa Mazars [a], Erick Ringot [a, b]

[a] LMDC, INSA/UPS Génie Civil, 135 Avenue de Rangueil, 31077, Toulouse Cedex 4, France
[b] LRVision SARL, 13 Rue du Développement, 31320, Castanet-Tolosan, France

ARTICLE INFO

Keywords:
Circular economy
Photocatalysis
Nitric oxide
Titanium dioxide
Hexafluorotitanates
Mortar

ABSTRACT

Titanium metal is widely used in the aeronautical sector for its specific properties and corrosion resistance. The design of titanium workpieces is based on chemical milling: a fast, precise, low cost technique popular in the aerospace industry. Material is removed from selected areas of a part by immersing it in a strong chemical reagent. This process produces shallow cavities on plates and sheets or removes shallow layers of materials from large aircraft components to optimize the strength/weight ratio. However, it leads to large volumes of wasted acid baths, which are harmful to the environment and have to be sent to an approved waste facility. The objective of this paper is to highlight a cleaner production process based on the circular economy concept, i.e. reduce, reuse and recycle to limit environmental pollution and operating costs. Waste from chemical milling baths used in the design of titanium parts was recovered with the aim of synthesizing titanium dioxide and using it for air depollution applications. The waste consisted of hexafluorotitanate compounds. Various processing techniques to synthesize titanium dioxide from hexafluorotitanate compounds were tested and resulted in powders having different physicochemical characteristics. The synthesis parameters studied were the nature of the decomplexing agent, the dehydration temperature and the heating period. Photocatalytic coatings were then formulated on the basis of the synthesized powders. They were applied to a mortar surface to evaluate their efficiency to degrade nitric oxide under two UV lighting intensities, 5 and 20 W/m^2. Depending on the synthesis process conditions, the concentration and crystal form of titanium dioxide particles varied, leading to more or less efficient photocatalytic coatings. The proportions of anatase and rutile phases in the synthesized powders were between 3 and 13%, and 5 and 30%, respectively. Concerning the particle size distribution, the variations observed were dependent on the D values. $D_{10\%}$ was quite similar for all powders. However, $D_{50\%}$ and $D_{90\%}$ differed by a factor of two for some powders, notably because of the presence of impurities or remaining decomplexing agent particles. NO degradation varied depending on the photocatalytic dispersions and could reach 7% under an irradiation of 20 W/m^2. This article highlights the possible valorization of a massive industrial waste for specific applications provided that the conditions of processing techniques are optimized.

1. Introduction

Chemical milling is used in various industries, such as aerospace, electronics and automotive manufacturing to shape common metal parts (made of aluminium, stainless steel and titanium) and respect detailed structural design, which is not feasible by mechanical methods (El Hofy, 2005). By controlled dissolution with a strong reagent, called the etchant, this process allows complex shapes, accurate geometries and reduced thicknesses to be obtained. The metal is removed only at certain locations of the workpiece surface thanks to special protecting coatings, called maskants. More specifically, in the aerospace industry, chemical milling is widely used to reduce the weight of aircraft parts by selectively removing precise volumes of material (Harris, 1976). The process was first applied industrially, notably by North American Aviation, Inc. (California, USA), to etch aluminium components for rockets. It was patented in 1956 (Sanz, 1956). Etchants, which may be acid or

* Corresponding author.
E-mail address: hot@insa-toulouse.fr (J. Hot).
[1] Present address: CIRIMAT, Université de Toulouse, UPS, 118 Route de Narbonne, 31062 Toulouse cedex France.

https://doi.org/10.1016/j.jclepro.2019.119344

alkaline solutions depending on the materials to be etched, are the most influential parameter in the chemical milling (Çakır, 2016, 2008; Tehrani and Imanian, 2004). Some of them are summarized in (Çakır et al., 2007). For example, ferric chloride ($FeCl_3$) is a widely used etchant for iron, copper and aluminium based alloys, and cupric chloride ($CuCl_2$) is used for etching copper and its alloys. In the case of titanium alloys, the chemicals involved in the process include hydrofluoric acid (HF), an acid from the group comprising hydrochloric acid, nitric acid (HNO_3) or sulfuric acid, and surface tension reducing agents (Chen, 1990). Etching titanium with HF alone is a slow process, which produces hydrogen gas and leads to a rough surface finish (Tal Gutelmacher and Eliezer, 2004). Titanium reacts with HF according to reaction (1).

$$2\ Ti + 6\ HF \rightarrow 2\ TiF_3 + 3\ H_2 \quad (1)$$

The use of HNO_3 reduces hydrogen absorption by titanium alloys and produces a smoother surface. The weight ratio HNO_3/HF defines the etching rate. If the HNO_3 concentration is too high (HNO_3/HF > 10), the resulting etching rate will be slow ($\approx$2.5 μm/min). On the other hand, if the HF concentration is high (HNO_3/HF < 10), the etching will be fast and uneven ($\approx$18 μm/min) (Markle, 2015a, 2015b). When a mixture of HF and HNO_3 is used, reactions (2) and (3) occur.

$$Ti + 2\ HNO_3 \rightarrow TiO_2 + 2\ HNO_2 \quad (2)$$

$$TiO_2 + 6\ HF \rightarrow H_2TiF_6 + 2\ H_2O \quad (3)$$

The overall reaction for titanium etching in mixed acids is

$$3\ Ti + 18\ HF + HNO_3 \rightarrow 3\ H_2TiF_6 + 9/2\ H_2 + NO + 2\ H_2O \quad (4)$$

In addition to the type of acids and their concentrations, temperature and time are also considered as influencing factors. Chrcanovic and Delany (2014) showed that the surface roughness of titanium treated with acidic solution increased with temperature and time. The same was true for Marsuhashi and Takahashi (2002), who observed an increased loss of titanium by corrosion. Therefore, it is important to control the etching conditions. Moreover, the ingredients in the bath require frequent analysis and adjustment. The etching rate is dependent on the free concentration of HF, which decreases through time due to changes in the surface layer and in the composition of the etching solution. As the titanium ion concentration increases with time in the bath, HF is consumed by the formation of anionic titanium fluoride complexes TiF_6^{2-} and the chemical pickling efficiency decreases (Schneiker and Forsberg, 2014; Sutter and Goetz Grandmont, 1990). To combat the increasing titanium concentration, periodic additions of HF can be made to the bath to prolong its life until it becomes inefficient. In this case, wasted acid baths must be sent to an approved waste facility as they can be very harmful for the environment (Public Health England, 2018; 2017). To avoid a long and expensive waste handling process, several researchers have investigated the possibility of restoring the bath by using a chemical reaction (Bares and Cros, 2010) or thermal process (Baillon Martin et al., 2004) to precipitate excess titanium in the form of hexafluorotitanate compounds.

In Toulouse, France, SATYS ST PRODEM is a company specializing in the chemical milling of titanium parts for the aerospace industry. A specific process under patent is followed by SATYS ST PRODEM to regenerate a nitrohydrofluoric bath for chemical etching of parts made of titanium or titanium alloy in order to reduce the inputs of chemicals (54% for HF and 90% for HNO_3) and water (88%), the volume of waste and the operating costs (90%), and to increase productivity. These objectives are notably identified by Gusmerotti et al. (2019) as being the main drivers (economic and environmental) of circular economy. One step of this regeneration process precipitates titanium out of chemical baths to obtain hexafluorotitanate compounds (Nicolas, 2018). This invention was part of the RUTILE project (2016–2019), which, in addition to innovative process development, also studied the valorization of titanium (in the form of hexafluorotitanates) from chemical milling baths to titanium dioxide (TiO_2) for air depollution applications. The experimental research work presented in this paper deals more specifically with the latter point and focuses on the development of photocatalytic coatings to be applied to building materials. It shows an example of a circular economy business model based on resource recovery, where the waste of one company (aerospace sector) could be used as a resource by another (construction sector) (Suárez Eiroa et al., 2019). Photocatalytic materials containing TiO_2 have indeed received growing interest during recent decades (Agrios and Pichat, 2005; Fujishima and Zhang, 2006). They have proven to be efficient in air (Ângelo et al., 2013) and water purification (Fatima et al., 2019) and have shown self cleaning (Pozo Antonio and Dionísio, 2017) and antibacterial properties (Verdier et al., 2014). A recent review by Ren et al. (2017) on the use of photocatalytic materials to purify air discusses material design strategies aimed at improving their performance. The authors notably report techniques to improve the efficiency of photocatalysts under visible light, such as ion doping, nonmetal ion doping, and metal semiconductor heterojunctions. Several other studies have dealt specifically with the application of this kind of coatings to building materials to degrade nitrogen oxides (NO_x) and Volatile Organic Compounds (VOCs). For example, Hot et al. (2017) showed that the NO photocatalytic degradation was dependent on the substrate roughness and the quantity of functional coating applied to the surface. Martinez et al. (2014, 2012, 2011) particularly studied the photocatalytic coatings for construction materials and the parameters that controlled their performance to degrade NO and BTEX. In Martinez et al. (2014), the authors highlighted the improved photocatalytic performance of coated mortar compared to glass because of its absorption capacity and showed the absence of humidity influence for initial concentrations between 0.4 and 1 ppm. Yamamoto et al. (2014) reported a 48% decrease in toluene concentration attributed to the photooxidation reaction occurring at the surface of TiO_2 coated building material.

The photocatalytic process widely reported in the literature consists of four main steps, as shown in Fig. 1: ① under irradiation, electrons rise from the valence band to the conduction band leaving electron holes; ② the electron hole pairs produced reach the surface of the semiconductor particles; ③ through reactions with the adsorbed oxygen and water coming from the surrounding air, reactive oxygen species such as $HO^{\bullet}$, $O_2^{\bullet -}$ and $HO_2^{\bullet}$ are created; ④ pollutants are decomposed or mineralized through a reduction oxidation process. Lasek et al. (2013) especially discussed the main processes leading to the removal of NO_x by photocatalysis. Among them, the NO photo oxidation for TiO_2 photocatalysts led to HNH_3 via the formation of HNO_2 and NO_2. Huang et al. (2016) focused on the reactions occurring during the photocatalytic oxidation of typical indoor VOCs and formaldehyde. The complete oxidation should lead to CO_2 and H_2O.

In this paper, the nitric oxide (NO) photocatalytic oxidation over TiO_2 based semiconductor resulting from waste was studied. Mortar surfaces were coated with TiO_2 based dispersions in water synthesized from hexafluorotitanate compounds. In the RUTILE project, the INEOSURF company was in charge of the synthesis step to obtain TiO_2 particles. According to the synthesis process conditions, the resulting TiO_2 particles had various physicochemical characteristics leading to photocatalytic dispersions that were

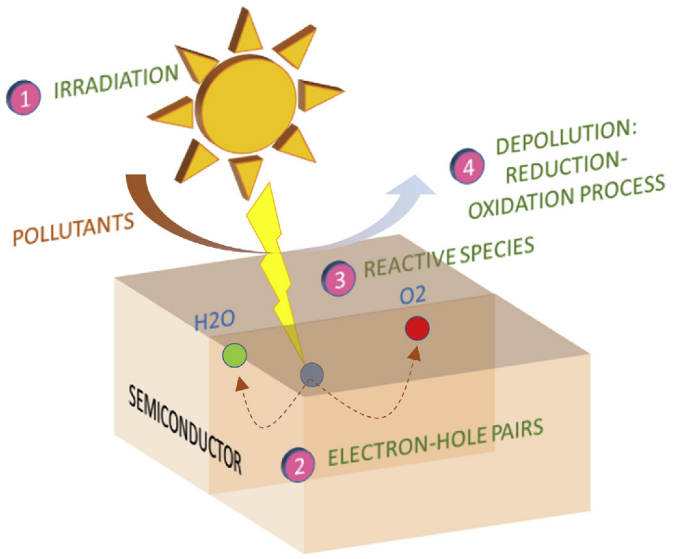

Fig. 1. Schematic representation of the photocatalysis process on semiconductor surface showing the 4 main steps: irradiation, electron-hole pairs reaching the surface, reactive species creation, and depollution by reduction-oxidation process.

more or less efficient to degrade NO. The authors investigated the influence of the synthesis conditions, particularly on the crystal form of TiO_2 and its proportion in the synthesized powders, and on the particle size. Air depollution tests were conducted at lab scale using a reactor. Pure dilute NO (stabilized in nitrogen) was continuously injected as the gaseous pollutant, and NO and nitrogen dioxide (NO_2) concentrations were measured with a nitrogen oxide (NO_x) analyzer. By comparing the NO inlet and outlet concentrations, NO abatements were evaluated for all the experiments conducted. The depollution efficiency of photocatalytic dispersions based on TiO_2 resulting from hexafluorotitanate compounds were then compared.

2. Materials and methods

2.1. Substrate

A common building material, mortar, was used as the substrate. Normalized mortar samples with a water/cement ratio of 0.5 (W/C 0.5) were prepared according to the European standard NF EN 196−1. Mortar was composed of siliceous sand (grain size 0−2 mm) and CEM I 52.5 Portland cement. The preparation was carried out at ambient temperature and a relative humidity of 55%. Each sample was mechanically mixed and then cast in a 30 × 30 × 1 cm^3 steel mold with the aid of a vibrating table. The resulting slab was kept covered in a room at constant temperature and humidity. It was demolded after 7 days and sawn into 10 × 5 × 1 cm^3 samples. Mortar samples were finally ground (120 μm abrasive sandpaper) before photocatalytic dispersion was applied to the surface. The appearance of the mortar surface is shown in Hot et al. (2017).

2.2. TiO_2 based powder synthesis

TiO_2 is an inorganic photocatalytic semiconductor. Because of its excellent light scattering properties, its primary application is as a white pigment in paints, foods, cosmetics, toothpastes or polymers to provide white opacity and brightness (Fisher and Edgerton, 2001). Moreover, this semi conductor has been studied for at least three decades for its photocatalytic ability, especially in the fields of energy, environment, construction and biomedicine. For example, Cassar (2004) discussed the air depollution and self cleaning properties of TiO_2 loaded cementitious materials and notably highlighted the synergy between cement and TiO_2. Hot et al. (2017, 2016) and Topalov et al. (2019) investigated the effectiveness of photocatalytic coatings to degrade NO and NO_2. They carried out experiments with various building materials (mortar, wood, plasterboard) at laboratory scale and in a 10 m^3 experimental chamber. Gholami et al. (2017) studied the effect of TiO_2 based nanocoatings for solar cell applications and observed a decrease in the accumulation of dust on coated glass samples. Verdier et al. (2014) focused on the antibacterial activity of TiO_2 on Escherichia coli bacteria and the parameters that influenced its inactivation by photocatalysis.

Three TiO_2 crystalline forms exist in nature: anatase, rutile and brookite. Rutile is stable, while anatase and brookite are metastable, but anatase shows a better photocatalytic activity than rutile and brookite because of its higher gap energy (3.02 eV for rutile, 3.14 eV for brookite and 3.23 eV for anatase). Anatase transforms irreversibly to rutile at elevated temperatures. However, this transformation can be promoted at lower temperatures or even inhibited depending on numerous parameters, as reported by Hanaor and Sorrell (2011). In the literature, different synthesis methods are reported for obtaining TiO_2 in various forms (amorphous, anatase, rutile or anatase rutile mixture). Common synthesis methods of TiO_2 and the resultant phases are notably summarized in Hanaor and Sorrell (2011). Arroyo et al. (2002) and Liu et al. (2009), for example, both used $Ti[OCH(CH_3)_2]_4$ as precursors. The first authors performed a sol gel synthesis at room temperature using metal ion dopants (Mn^{2+}) to pass from amorphous TiO_2 structure to crystalline TiO_2 phases. The other authors dissolved $Ti[OCH(CH_3)_2]_4$ into a solution containing isopropyl alcohol and sucrose, which was then heated for 12 h at 160 °C in order to obtain semi crystalline TiO_2. Two calcination steps were finally carried out: first in a nitrogen atmosphere for 4 h at different temperatures and then in an oxygen atmosphere for 3 h at 700 °C. Zhang and Tang (2018) achieved titanium sulfate hydrolysis at room temperature in order to obtain hydrous amorphous TiO_2 particles, which were then calcined for 2 h at various temperatures to form pure anatase and rutile phases, and a mixture of both. A deposition method is also reported in the literature as a means to obtain TiO_2 coating on a substrate. Chemical vapor deposition (CVD), for example, was investigated by Mills et al. (2002). A TiO_2 film was prepared on glass via the reaction of $TiCl_4$ with ethyl acetate. The photo induced superhydrophilic and photocatalytic activities of this film were then assessed. Physical vapor deposition (PVD) was studied by Meyer et al. (2004) to generate photoactive TiO_2 films on titanium metal substrates by using an electrochemical process of anodic spark plasma.

In the present paper, the TiO_2 based powders studied were obtained from waste resulting from chemical milling baths of the aeronautical industry. This waste consisted of hexafluorotitanates (TiF_6 compound) in which Ti was present as Ti^{4+}. It was provided by SATYS ST PRODEM to INEOSURF, which then conducted various syntheses to transform it into TiO_2. The synthesis was characterized by two main steps: (1) transformation of hexafluorotitanates into $Ti(OH)_n$ by using decomplexing agents, and (2) $Ti(OH)_n$ dehydration to obtain TiO_2 crystalline phases. Different decomplexing agents and dehydration temperatures were tested. The role of the decomplexing agents was to release fluoride ions from TiF_6 compound. Among them, a weak base was used to promote $Ti(OH)_n$ formation, and Ca based mineral compound was added to precipitate fluoride ions from solution as calcium fluoride (CaF_2). The synthesis conditions for the samples tested are presented in Table 1. For samples 1A and 1B (respectively samples 3A and 3B), the synthesis was carried out with the same weak base and

Table 1
TiO_2-based powder synthesis conditions: reference sample, decomplexing agent, dehydration temperature and time period are specified.

Sample	Decomplexing agent	Dehydration temperature (°C) and time period (h)
1A	Weak base	650 °C for 3 h
1B	Weak base	650 °C for 3 h
2	Weak base and Ca-based agent	550 °C for 3 h
3A	Weak base and Ca-based agent	650 °C for 3 h
3B	Weak base and Ca-based agent	650 °C for 3 h
4	Si-based and Ca-based agents	550 °C for 3 h
5	Si-based and Ca-based agents	650 °C for 3 h
6	Ca-based agent	550 °C for 3 h
7	Ca-based agent	650 °C for 3 h

dehydration temperature. However, for sample 1A (respectively sample 3A), the initial quantity of waste to be transformed (i.e. hexafluorotitanates) was larger (5 times more) and a smaller quantity of weak base was used as the decomplexing agent (reduction of 23% between samples 1B and 1A, respectively samples 3B and 3A). The pH was measured during the synthesis and depended on the decomplexing agent added. For samples 1A and 1B, the pH was 10 ± 0.5 due to the weak base in excess. For other samples, as a strong base was used (Ca based agent), more OH^- ions were released (concentration above 10^{-2} mol/L) leading to a higher pH value, around 12 ± 0.5.

Dehydration temperature played an important role in the formation of TiO_2 crystalline phases. However, due to the use of different processing methods (especially in terms of kinetics) and raw materials (fineness and purity), the phase transformation temperature between anatase and rutile was hard to define. Various transition temperatures have been reported in the literature. They are summarized in (Hanaor and Sorrell, 2011). The reported transition onset temperatures of the anatase to rutile transformation in bulk pure anatase in air appeared to converge around 600 °C. For example, Jamieson and Olinger (1969) gave a diagram illustrating the reaction boundaries of phase transitions in TiO_2 according to pressure and temperature values. These authors showed that anatase to rutile phase transformation started around 480 °C and finished at 600 °C. Arroyo et al. (2002) reported that anatase to rutile transformation occurred between 600 and 750 °C for pure TiO_2 materials. In the case of our study, the influence of dehydration temperature on TiO_2 crystalline phase formation was also observed. The diffractograms in Fig. 2 show that, for the same synthesized powder, compounds appeared or disappeared in various proportions under different dehydration temperatures. The crystalline phases of interest are referred as "A" for Anatase and "R" for Rutile. They were respectively identified at 550 °C and 650 °C. At 450 °C, no crystalline form of TiO_2 was detected.

2.3. Photocatalytic dispersion preparation and coating application

Each photocatalytic dispersion was prepared as follows: 5 g of TiO_2 based powder was mechanically dissolved using a stirring blade during 5 min in 100 ml of distilled water solution containing 3.5 g of dispersant (Borchi® Gen 1252) and 0.1 g of antifoaming agent.

The dispersion was applied to the mortar surface using a fine brush. The quantity of TiO_2 based dispersion on the surface was determined by weighing the recipient containing the dispersion and the brush before and after coating the mortar sample. The TiO_2 quantity (dry content) on the surface was then evaluated by considering the proportions of anatase and rutile phases in the dried synthesized powder (values obtained from X Ray Diffraction (XRD) analyses). Between 2 and 3 layers of dispersion were applied to each surface. The surface was allowed to dry at ambient temperature and humidity for 30 min after each application. The final TiO_2 dry content applied to each mortar surface (expressed in g/m^2) before depollution tests were conducted is indicated at the top of each bar in Fig. 8.

2.4. TiO_2 based powder characterization

2.4.1. XRD

A Bruker D8 Advance diffractometer (copper anode) was used to identify the chemical composition of powders. Two software tools were employed: one for compound identification (qualitative results with EVA software), and the other for quantification by the Rietveld method (TOPAS software). However, the TOPAS database was not sufficiently extensive to evaluate all of the compound proportions in the synthesized powders so, to obtain quantitative results in the framework of this study, an analytical procedure based on X ray diffraction intensities was used. This kind of method has already been reported in the literature. Spurr and Myers (1957)

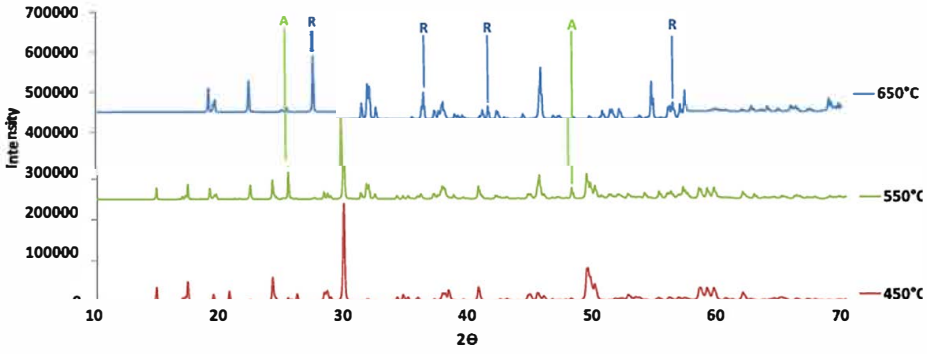

Fig. 2. Diffractograms obtained for the same synthesized powder dehydrated at three different temperatures: 450 °C, 550 °C and 650 °C ("A" for Anatase and "R" for Rutile): increasing temperature led to anatase to rutile transformation.

and Serna et al. (2014) plotted a calibration curve to evaluate the relative quantities of anatase and rutile in mixtures containing only TiO_2 by plotting the intensity ratio (I_A/I_R) as a function of the weight ratio (w_A/w_B) ($_A$ for anatase and $_R$ for rutile). As the powders tested in this study contained many impurities, two calibration curves were needed: one for the anatase phase and the other for the rutile phase. Therefore, mixtures of pure anatase (Prolabo commercial product from RECTAPUR®) and rutile (commercial product KRONOS®2310) were prepared. The following compositions were investigated to establish the calibration curve for each phase: 100% anatase, 80% anatase +20% rutile, 60% anatase +40% rutile, 40% anatase +60% rutile, 20% anatase +80% rutile, and 100% rutile. Each composition was homogenized using ten 6 mm glass balls for 3 min and then ground and sieved with an 80 µm mesh for XRD analyses.

Peak intensities at characteristic 2Θ values were collected from the resulting diffractograms: 25.3° and 48.0° for anatase, and 27.4° and 36.1° for rutile (Guimaraes et al., 2016; Hanaor and Sorrell, 2011). Intensity was then plotted versus each phase proportion in order to obtain the two calibration curves shown in Fig. 3. These calibration curves allowed the anatase and rutile phases in the powders studied to be quantified. Peaks at 48.0° and 27.4° were respectively chosen for anatase and rutile phases because of the better linearity of the calibration curves (higher R^2 coefficient values).

2.4.2. Granulometry

The CILAS1090 laser particle size analyzer was used (according to ISO 13320). This kind of analyzer offers a wide range of particle size measurements. The technique is based on laser light diffraction: the particle size is specified from the light intensity distribution pattern by using the Fraunhofer diffraction theory relationship. Before carrying out particle size analyses, powders were ground and sieved with an 80 µm mesh. The following values were compared: average diameter, $D_{10\%}$, $D_{50\%}$ and $D_{90\%}$. The $D_{50\%}$ (the median) was the size in microns that split the distribution with half above and half below this diameter. Similarly, 90% and 10% of the distribution were below the $D_{90\%}$ and $D_{10\%}$ diameters respectively.

2.4.3. SEM/EDS

Scanning electron microscopy (SEM) was used to investigate the microstructure of TiO_2 based powders. The analyses were conducted with a JEOL KSM 7800F Prime instrument (voltage of 5 and 10 kV). As the image resolution was sufficient, it was not necessary to metallize the powders. Images in LED (Lower Electron Detection, information on morphology and relief) and UED (Upper Electron Detection, better resolution but poor relief) modes were obtained using secondary electrons. Images in COMPO mode (for composition) were acquired using backscattered electrons. These electrons are sensitive to the atomic number of elements: the heaviest atoms re emit more electrons than lighter atoms. Zones formed by elements having a high atomic number thus appear brighter. Further analyses were conducted by Energy Dispersive Spectroscopy (EDS). Combined with SEM, EDS was used to determine the elementary composition of individual points or to show the overall distribution of elements in the analyzed powders by cartography. Magnifications used were between x250 and x30 000.

2.5. Experimental setup for air depollution test

Various gaseous pollutants can be eliminated by the photocatalytic TiO_2/cement system (e.g. NO_x, SO_x, VOCs). In this paper, the degradation of NO by photocatalysis was especially studied. The overall process is well documented in the literature and can be briefly described as follows: NO present in the air is oxidized when TiO_2 photocatalyst is exposed to light at wavelengths around and less than 388 nm. Through intermediate steps, including NO_2 generation, NO is finally converted to nitrate by means of a reduction oxidation process. The performance could be enhanced depending on experimental and physicochemical parameters such as irradiance, dopant and substrate. Bloß and Elfenthal (2007) reported that doping TiO_2 with carbon led to a shift in the cut off wavelength (from 388 nm to 535 nm), which increased its efficiency to degrade NO under UV and visible light. Horgnies et al. (2012) highlighted the influence of substrate by showing the absorption capacity of concrete. Hüsken et al. (2009) observed the dependence of the NO degradation rate on the irradiance.

The setup used to assess the efficiency of photocatalytic materials (i.e. mortar samples covered with photocatalytic dispersions prepared from TiO_2 based powders) is described in (Hot et al., 2017). It was inspired by ISO 22197−1 and XP B44001 standards. The experimental setup was placed in an air conditioned room at 20 ± 1 °C with relative humidity (RH) between 30 and 44%. An air generator (Environnement S.A., France, model ZAG7001) filtered the ambient air, which was then humidified and mixed with pure NO pollutant coming from a gas cylinder (8 ppm, pure NO stabilized in nitrogen, Air Liquide, France). Air and NO flow rates were

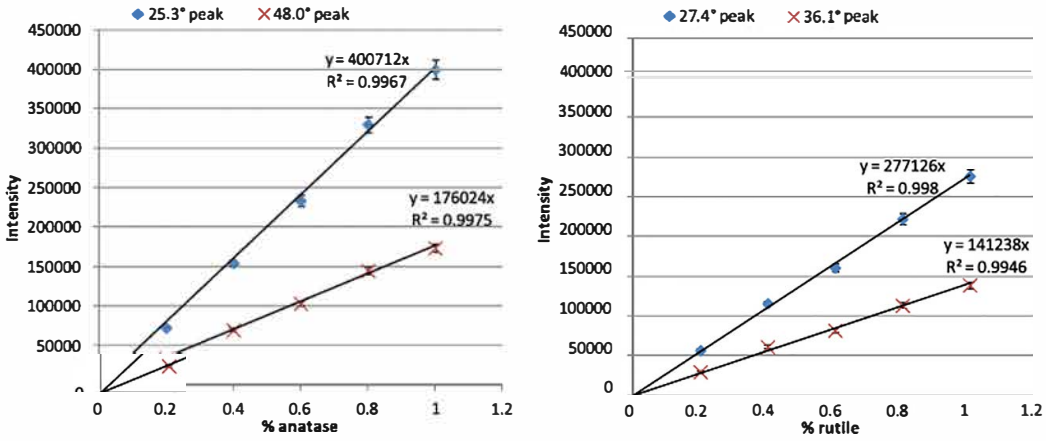

Fig. 3. Anatase calibration (left) and rutile calibration curve (right): peaks at 48.0° and 27.4° were chosen for anatase and rutile phases, respectively, because of the better linearity (higher R^2 values). These calibration curves were used for the quantification of anatase and rutile phases in the powders studied.

controlled with mass flow controllers. The diluted polluted air (initial NO concentration equal to 400 ppb after dilution with air) flowed continuously through the reactor. NO_x concentrations were measured by a chemiluminescent analyzer (Environnement S.A., France, model AC32M), which displayed NO, NO_2 and NO_x concentrations.

The steps of the experimental protocol are represented in Fig. 4: NO concentration was first measured when the polluted air went through the bypass for 10 min in darkness (light OFF), then 10 min inside the reactor with the mortar sample in darkness and, finally, 10 min inside the reactor with the mortar sample under UV light (light ON). Lighting intensity on the upper surface of the reactor was measured using a Gigahertz Optik radiometer equipped with a detector for UV A wavelengths (UV 3717 model, 315–400 nm). Three bulbs (UV light CroLED®, 365 nm) were used for the lighting system. They were placed at two different heights (i.e. distances between the lighting source and the upper surface of the reactor) of 15 cm and 45 cm, to obtain two different light intensities on the upper surface of the reactor: 20 W/m^2 and 5 W/m^2 respectively. These high UV intensity values were chosen to promote the NO removal efficiency. This protocol was also carried out with no mortar sample in the reactor (empty reactor) and with reference mortar (uncoated) to evaluate the respective effects of the UV light (i.e. photolysis) and the mortar matrix (i.e. adsorption/absorption) on NO concentration (cf. part 3.2.1). In Fig. 4, the NO concentration decrease followed by the increase occurring at around 10 min was associated with the filling of the reactor.

3. Results and discussion

3.1. Physicochemical characterization of TiO_2 based powders

3.1.1. XRD

Anatase and rutile phases exhibit characteristic diffraction peaks at specific 2Θ values: 25.3° (101), 37.3° (004) and 48.0° (200) for anatase, and 27.4° (110), 36.1° (101) and 41.2° (211) for rutile (Fisher and Edgerton, 2001; Guimaraes et al., 2016; Hanaor and Sorrell, 2011). These peaks were used to identify the presence of TiO_2 crystalline forms in the synthesized powders. Their proportions were evaluated with the help of the calibration curves (at 48.0° peak for anatase phase and 27.4° peak for rutile phase), except for samples 1B and 3B, for which the Rietveld method was used (as these powders contained fewer impurities, it was possible to identify all the compounds using the TOPAS database, cf. part 2.4.1). The results are presented in Table 2. XRD patterns of the analyzed powders revealed the co existence of anatase and rutile for samples 1B, 3B, 4 and 5. Only rutile was identified for samples 1A, 2, 3A, 6 and 7.

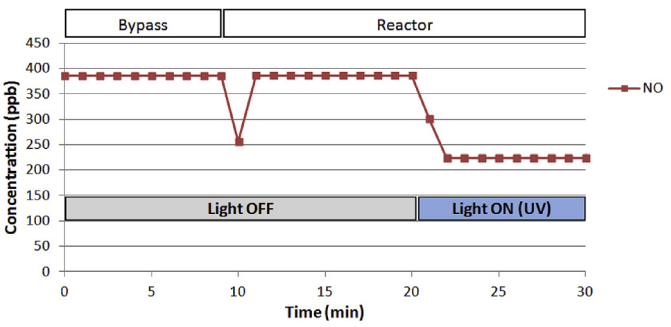

Fig. 4. Experimental protocol for assessing NO degradation. Expected NO concentration evolution during a test (theoretical representation) is shown. The first decrease was due to the filling of the reactor, the second one to photocatalytic activity when the light was switched on.

As stated in part 2.2, authors in the literature have reported different phase transformation temperatures depending on the process parameters and the characteristics of the raw materials (Hanaor and Sorrell, 2011; Zhang and Tang, 2018). As a general conclusion, the value of 600 °C can be kept in mind as the anatase to rutile transition temperature for pure anatase. However, according to the results shown in Table 2, this transition temperature seemed to be lower in this study. A comparison of samples 2 and 3A suggests that the increase in the dehydration temperature (550 °C–650 °C) led to a higher rutile proportion (5% vs. 9%) rather than to anatase formation. The same trend was observed for samples 6 and 7 (13% vs. 26%). For samples 4 and 5, both composed of anatase and rutile, the increase in rutile proportion from 17 to 25% (respectively the decrease in anatase proportion from 5 to 3%) with dehydration temperature (550 °C vs. 650 °C) showed that the temperature for which TiO_2 particles transformed to rutile was reached but was lower. Moreover, by comparing samples 1A and 1B (respectively 3A and 3B), the influence of waste and weak base proportions on crystalline phase formation was highlighted. Samples 1B and 3B had a higher proportion of crystallized phase due to a larger quantity of decomplexing agent. For the authors, the presence of impurities in the synthesized powders, leading to a change in the reaction boundaries of phase transitions in TiO_2, appeared to be a reasonable explanation. This phenomenon has been reported in the literature. Shannon and Pask (1965) summarized quantitative data on the effect of impurities on the transformation of anatase. In addition, these authors showed that the rate of the anatase rutile transformation and activation energy were governed by the nature and amount of impurities. They notably highlighted the inhibiting effect of fluoride ions and ions of valence greater than four such as sulfate (S^{6+}) and phosphate (P^{5+}) due to the reduction in the number of anion vacancies (substitution of two fluoride ions for an oxygen ion) and in the concentration of oxygen vacancies respectively. Arroyo et al. (2002) studied the effect of manganese ions on the anatase rutile phase transformation of TiO_2. They showed that significant structural changes occurred during the various stages of the phase transformation, depending on the manganese concentration: either stabilization of the anatase phase was observed or the rutile formation was favored. They also pointed out that the anatase rutile transformation temperature was lowered for the TiO_2 samples with the highest manganese concentration. Concerning the recovery of TiO_2, the percentage of crystallized phases varied between 5 and 43%, with the highest value obtained for sample 3B. In the authors' opinion, the chemical yield was low, which resulted in the presence of titanium fluoride complexes, such as TiF_6 and $TiOF_5$, in the synthesized products. Also, the dehydration time period was not optimal to dehydrate and crystallize $TiOH_4$ and thus led to the formation of anatase and/or rutile.

3.1.2. Granulometry

Particle size analysis was carried out for all the synthesized powders, except for samples 1B and 3B. The results are summarized in Table 3 (uncertainty was estimated to be ±2 μm for average diameter and ±0.4 μm for $D_{10\%}$). In general, nanometric TiO_2 particles improve the photocatalytic activity (Hanaor and Sorrell, 2011; Rambabu et al., 2016; Shannon and Pask, 1965). In this study, the diameters obtained were representative of micrometric powders. The specific surface area and therefore the reactive surface area of the synthesized powders were lower than expected, notably because of the presence of impurities. It can be noted that the $D_{50\%}$, $D_{90\%}$ and average diameter values for samples 4 and 5 were higher than for the others: between 3 and 5 times higher for $D_{50\%}$ and between 2.5 and 5.5 times higher for $D_{90\%}$. This difference could be explained by the type of decomplexing agent used during the

Table 2
Anatase and rutile proportions in the analyzed powders (grey shaded columns for dehydration temperature of 650 °C).

Sample	1A	1B	2	3A	3B	4	5	6	7
Dehydration temperature (°C)	650	650	550	650	650	550	650	550	650
Anatase (%)		3			13	5	3		
Rutile (%)	10	39	5	9	30	17	25	13	26

Table 3
Particle size distribution of the synthesized TiO_2-based powders (grey shaded columns for dehydration temperature of 650 °C): 10% of the distribution was below $D_{10\%}$, $D_{50\%}$ was the median size and 90% of the distribution was above $D_{90\%}$. Uncertainty was estimated to be ±2 μm for average diameter and ±0.4 μm for $D_{10\%}$.

Diameter (μm)/Sample	1A	2	3A	4	5	6	7
$D_{10\%}$	1.52	0.54	1.58	1.49	1.93	1.35	1.50
$D_{50\%}$	5.58	3.83	5.52	19.70	19.42	5.09	5.82
$D_{90\%}$	22.15	11.90	18.47	67.54	55.36	16.48	20.45
Average diameter	8.69	5.38	7.93	28.03	24.72	7.40	8.50

synthesis. An Si based decomplexing agent having particles with diameters between 0.06 and 0.2 mm was added, leading to powders (samples 4 and 5) with higher $D_{50\%}$, $D_{90\%}$ and average diameter values (19.70 μm, 67.54 μm and 28.03 μm, respectively, for sample 4). Therefore, $D_{10\%}$ reported in Table 3 were considered as the most representative diameter values for TiO_2 particles in the synthesized powders as the other ones were affected by impurities and decomplexing agents. $D_{10\%}$ values varied between 0.54 and 1.93 μm. A similar size range between 0.593 and 1.193 μm was reported by Hüsken et al. (2009) for commercially available standard TiO_2 in the anatase form. In addition, from results in Table 3, the particle sizes of powders dehydrated at two different temperatures (550 °C and 650 °C) were compared (sample 2 vs. sample 3A, sample 4 vs. sample 5, sample 6 vs. sample 7). It seemed that the synthesized powders dehydrated at 650 °C had higher $D_{10\%}$ values due to the presence of rutile phase (1.58 μm, 1.93 μm and 1.50 μm for samples 3A, 5 and 7 dehydrated at 650 °C, and 0.54 μm, 1.49 μm and 1.35 μm for samples 2, 4 and 6 dehydrated at 550 °C). This trend has been reported in the literature by several authors. Rambabu et al. (2016) reported a change of crystallite size of TiO_2 multi leg nanotubes annealed in air at temperatures ranging from 500 to 900 °C. They observed an increase in anatase grain size from 34 ± 2 nm to 46 ± 3 nm (corresponding to the peak (101)) during the process of phase transition from anatase to rutile upon heat treatment from 500 to 600 °C. As temperatures increased further, the transformation of anatase to rutile occurred and the average grain size corresponding to (101) plane of anatase and (110) plane of rutile was around 53 nm, 69 nm and 81 nm for samples annealed at temperatures of 700, 800 and 900 °C respectively. In addition, these authors highlighted a decrease in anatase grain size for high annealing temperatures, from 700 to 900 °C. As reported by Shannon and Pask (1965), this size reduction indicated a gradual transition of anatase to rutile due to the nucleation of rutile phase on the grain surface and spreading into anatase.

3.1.3. SEM/EDS

Fig. 5 shows SEM images of some synthesized powders. Specific shapes of compounds were noticed and were confirmed by EDS analyses: particles with a "stick" form were representative of the rutile crystalline phase, and octahedral particles were associated with anatase particles. TiO_2 crystalline phases were surrounded by amorphous phase (left) and spherical particles (right) were identified as fluorite (CaF_2), a phase formed when Ca based decomplexing agent was used for the synthesis. These observations were consistent with the literature, where research studies reported a more elongated shape for rutile particles due to a tetragonal prism structure. Anatase particles were found to be shorter with a tetragonal pyramidal structure (Hanaor and Sorrell, 2011; Ohno et al., 2002; Taguchi et al., 2003). As explained by Hanaor and Sorrell (2011), anatase and rutile crystal structures both consisted of TiO_6 octahedra with four edge sharing connectivity in anatase and two edge sharing connectivity in rutile. This specific three dimensional arrangement could explain the "stick" and "cubic" forms for rutile and anatase particles respectively. SEM and TEM (Transmission Electron Microscopy) images of rutile and anatase particles included in the TiO_2 powder were notably shown by Ohno et al. (2002) and Taguchi et al. (2003).

Fig. 6 shows silica particles observed for a powder synthesized with an Si based decomplexing agent. Their sizes were estimated to be around 100–150 μm (the size range of Si based decomplexing agent particles was 60–200 μm). This observation was consistent with particle size analysis results (part 3.1.2) showing higher diameter values for samples 4 and 5, which were attributed to the presence of silica particles. Lorencik et al. (2015) reported a similar SEM image showing the presence of micro scale particles that could be attributed to silica.

3.2. NO degradation

3.2.1. Photolysis and adsorption/absorption phenomena

Fig. 7 highlights a reaction between UV light and NO. When the reactor was empty (i.e. no mortar sample in it), a variation in NO concentration was observed at the dark/UV light transition. It could be attributed to a chemical process due to light, called photolysis (or photodecomposition). This kind of phenomenon has been reported in the literature for various compounds. For example, Silva et al. (2006) suggested that direct photolysis of azo dyes under UV light should not be ignored. In a different field, Kalinovskaya et al. (2016, 2011) showed that photolysis could improve the luminescent and photochemical characteristics of light transforming polymer materials, depending on their compositions and, notably, on the dopant used. The mechanism that describes the photodecomposition of NO was notably discussed in (McGee and Heicklen, 1964) and leads to the production of NO_2. Therefore, NO gaseous pollutant concentration in the reactor was probably affected by UV light during the experiments carried out in this study. As shown below, this impact was taken into account.

Moreover, by comparing the "NO empty reactor" and "NO uncoated mortar" curves in Fig. 7, a reaction between NO and mortar substrate was observed, leading to a slight decrease in NO concentration. It could be attributed to the adsorption/absorption phenomenon. Horgnies et al. (2012) demonstrated that concretes could continuously absorb a significant fraction of NO_2 (and, to a far lesser extent, NO) from the surrounding atmosphere over long periods, probably because of a reaction with strongly alkaline cement hydrates. In addition, Cassar (2004) highlighted the synergistic effect of the photocatalyst/cementitious matrix composite through adsorption by the hydroxides present in the cement matrix. According to him, the cement matrix effectively trapped NO_2 (which was generated through an intermediate step), together with nitrate salt formed during the photocatalytic oxidation of NO.

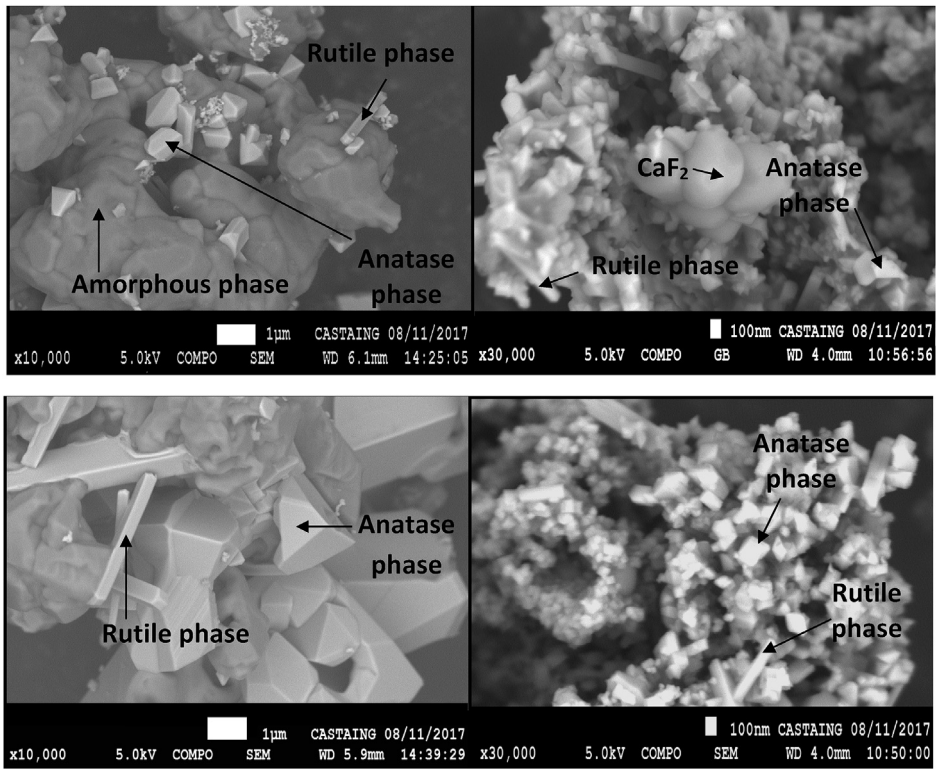

Fig. 5. Sample 1B (magnification x10 000) on the left and sample 5 (magnification x30 000) on the right. Particles with a "stick" form were representative of rutile crystalline phase and "cubic" shapes were associated with anatase particles.

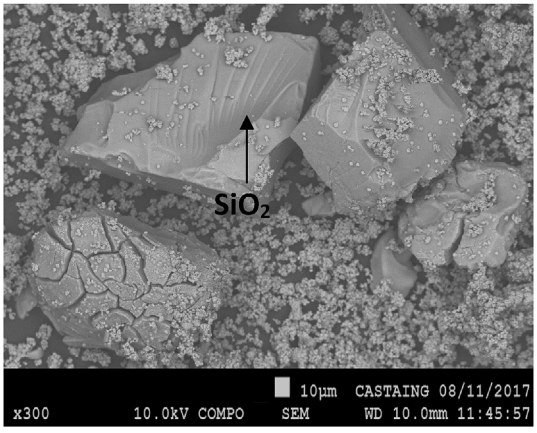

Fig. 6. Silica particles observed with SEM (magnification x300) for a powder synthesized with an Si-based decomplexing agent (SiO_2 particle size around 100 150 µm).

In addition, during the depollution tests carried out in this study, a generation of NO_2 was measured. This phenomenon was previously observed by Hot et al. (2017) when tests were conducted with mortar and wood samples coated with a TiO_2 based dispersion. As reported by other authors (Gauvin et al., 2018; Laufs et al., 2010; Martinez et al., 2011), this was an intermediate step expected to occur during NO photocatalytic degradation. NO_2 production and release can be limited depending on the substrate properties. Gauvin et al. (2018) showed that autoclaved aerated concrete released a higher quantity of NO_2 than wood wool cement board because of its closed pore structure. Hot et al. (2017) observed that, for the same quantity of TiO_2, NO_2 generation on mortar was half that seen on wood, which is consistent with the capacity of concrete to absorb NO_2 highlighted by Horgnies et al. (2012).

3.2.2. Abatement results

Fig. 8 shows the abatement values obtained with the photocatalytic dispersions prepared from the synthesized powders applied to mortar surfaces. At the top of each bar, the quantity of TiO_2 (dry content) applied to the surface is specified for each sample. The results for two lighting intensities (5 W/m^2 and 20 W/m^2) are compared. Under UV light, TiO_2 generates charge carriers (electrons and holes), which produce active radicals leading to the convertion of NO to adsorbed nitrate species via the formation of NO_2. As mentioned previously, the interaction of NO with light and a mortar matrix could lead to overestimated abatement values. Therefore, the abatement value obtained for the reference mortar (i.e. uncoated mortar) is also plotted for the two lighting intensities tested to show that the mortar matrix itself (adsorption/absorption) and mainly the light (photolysis) contributed to the decrease in NO concentration. The abatement for each coated mortar sample is expressed as a percentage (NO^{deg}(%)) and calculated according to equation (5):

$$NO^{deg}\ (\%) \quad 100 \times \frac{[NO]_{in} \quad [NO]_{out}}{[NO_x]_{in}} \tag{5}$$

where $[NO]_{in}$ and $[NO_x]_{in}$ are the inlet concentrations in the dark once the stable regime is established and $[NO]_{out}$ is the stable average outlet concentration measured during the illumination period.

By comparing NO degradation results obtained under 5 W/m^2 and 20 W/m^2, it can be noted, as expected, that the NO degradation was higher under 20 W/m^2 (Fujishima and Zhang, 2006). The same trend was observed by the authors in a previous study (Hot et al., 2017). Increasing the UV light intensity leads to the generation of a larger number of photons and consequently to the formation of more electron hole pairs. However, it was difficult to conclude on

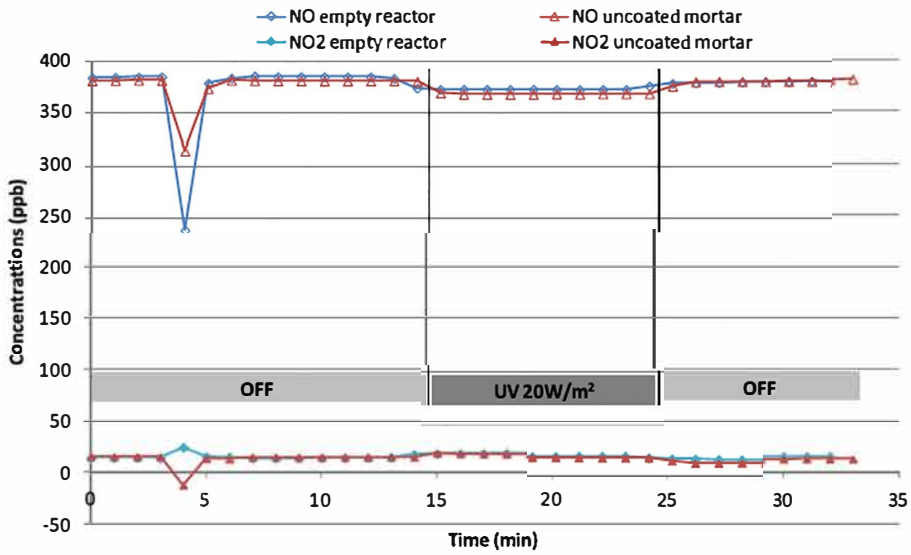

Fig. 7. NO_x (NO and NO_2) concentration evolutions (in darkness and with UV light 20 W/m^2) when the reactor was empty (without mortar sample) or with uncoated mortar inside (reference mortar without dispersion on the surface): a slight decrease in NO was observed due to photolysis and adsorption/absorption phenomena. Measurement uncertainty was estimated to be 1%.

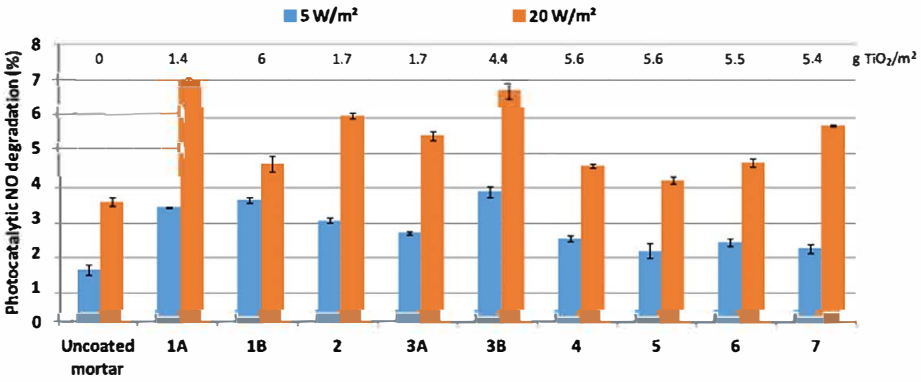

Fig. 8. NO degradation results obtained for the reference mortar (without dispersion on the surface) and mortars coated with the photocatalytic dispersions prepared from the synthesized powders under two lighting intensities 5 W/m^2 and 20 W/m^2. The TiO_2 dry content applied to each surface (g/m^2) is specified above the bars.

PROJET COFINANCÉ PAR LE FONDS EUROPÉEN DE DÉVELOPPEMENT RÉGIONAL

Fig. 9. European Union and Occitanie Region logos ("Project co-funded by the European Regional Development Fund").

the depollution function of the dispersions tested. The reasons were twofold: (1) the abatement values obtained were not sufficiently significant compared to the ones reported for the reference mortar, and (2) the quantity of TiO_2 applied to mortar surfaces was not easy to adjust, as the TiO_2 concentrations in the photocatalytic dispersions prepared from the synthsized powders were low (low dry content). Samples 1A and 3B seemed to be the most efficient. The maximum NO degradation obtained for these samples was around 7%, which is quite low compared to commercial products. This may have been due to the amount of dry TiO_2 on the mortar surface, which was not optimized for some samples. However, the authors think that the origin of the poor photocatalytic performance observed lay in the purity, size and morphology of the TiO_2 particles synthesized (Lorencik et al., 2015; Ren et al., 2017). As pointed out previously, the particles of the synthesized powders were of micrometric size. In this case, the surface area was small relative to the volume, resulting in fewer surface active sites at which photocatalysis was initiated through the adsorption of O_2 and H_2O and the action of light. It should also be kept in mind that photocatalytic dispersions studied in this paper were prepared from synthesized powders resulting from waste, in the aim of valorizing it, and thus contained more than 70% of compounds other than TiO_2. As shown by SEM/EDS analyses, the anatase and rutile particles formed during the synthesis appeared to be surrounded by other phases, which were amorphous or crystallized depending on the decomplexing agent used for the synthesis and on the presence of impurities in the initial precipitate. The presence of these phases could reduce the relative contributions of the anatase and rutile crystal facets by making them inaccessible to light and unavailable for the adsorption of environmental species.

The low degradation efficiency observed could therefore be attributed to the photocatalytic activity of the particles being hin dered by the unwanted phases surrounding them. Further research work will be needed to improve the synthesis conditions in order to obtain a higher quantity of crystallized TiO_2, a better crystallization and distribution, and avoid or eliminate the formation of other phases as far as possible.

4. Conclusion

The results showed that the dehydration temperature played an important role in the formation of TiO_2 crystallized phases. The XRD analyses highlighted the preferential formation of rutile phase at 650 °C. Due to the presence of impurities, the transition tem peratures from amorphous phase to anatase and then to rutile were changed. The presence of rutile and anatase was clearly observed by SEM for several powders, each of these phases being charac terized by its specific shape. However, their proportions in the synthesized powders were low, notably for anatase, with a maximum value of 13% (39% for rutile). The percentage of crystal lized phases (anatase+rutile) varied between 5 and 43%. The par ticle size analysis revealed that the synthesized powders were micrometric: $D_{10\%}$ values varied between 0.54 and 1.93 μm and average diameters ranged from 5.38 to 28.03 μm. XRD and SEM/ EDS analyses showed the presence of other compounds, notably SiO_2 particles and amorphous phases, surrounding the anatase and rutile, depending on the dehydration temperature and decom plexing agent used during the synthesis. These observations were consistent with the low proportion of crystallized TiO_2 particles and the large particle size observed in the synthesized powders. Air depollution tests revealed limited photocatalytic efficiency. The poor NO degradation observed (a maximum of 7%) was due to the low proportion of TiO_2 crystallized in the synthesized powders, the grain size and morphology, and the presence of surrounding phases hindering the photocatalytic activity of TiO_2 particles. However, it showed that the photocatalytic response was positive. Further research work should be done to optimize the synthesis conditions in order to obtain better results in terms of TiO_2 concentration and therefore NO reduction.

The research work presented in this paper is an example of the circular economy concept. Projects such as this one are opening up promising perspectives from an environmental and economic point of view. A cleaner production of titanium parts for use in the aeronautical sector is taking shape through the pilot scale regen eration process implemented by the SATYS ST PRODEM company. Transferring this process to an industrial scale will mean a signifi cant reduction in the operating costs, volume of wasted acid baths and quantity of chemical agents employed. This cleaner production process could also benefit other industries, such as construction, and especially companies that design and produce various specialty chemicals for building materials. The valorization of part of the resulting waste, which was the object of this paper, constitutes a real opportunity to optimize the TiO_2 supply chain. It could allow TiO_2 to be produced locally at lower cost, and reused for environ mental applications, such as air depollution, in the form of a coating for building materials.

Credit author statement

Julie Hot: Conceptualization, Validation, Writing Original Draft, Writing Review & Editing, Project administration, Funding acquisition.

Ariane Dasque: Investigation, Validation, Visualization, Writing Original Draft.

Jivko Topalov: Investigation.

Vanessa Mazars: Resources, Validation, Supervision.

Erick Ringot: Validation, Writing Review & Editing, Supervi sion, Funding acquisition.

Declaration of competing interest

The authors declare that they have no known competing financial interests or personal relationships that could have appeared to influence the work reported in this paper.

Acknowledgments

The authors are grateful to the Occitanie Region and the Euro pean Regional Development Fund (cf. Fig. 9) for their financial support in the framework of the RUTILE project (EASYNOV Eco innovation 2016, 2016–2019) and to SATYS ST PRODEM (Mr. Mathieu Nicolas) and INEOSURF (Dr. Jérôme Frayret) for their collaboration. They thank the Raimond CASTAING Center (UMS 3623, Toulouse) for its expertise in micro characterization.

Appendix A. Supplementary data

Supplementary data to this article can be found online at https://doi.org/10.1016/j.jclepro.2019.119344.

References

Agrios, A.G., Pichat, P., 2005. State of the art and perspectives on materials and applications of photocatalysis over TiO2. J. Appl. Electrochem. 35 (7 8), 655 663. https://doi.org/10.1007/s10800-005-1627-6.

Ângelo, J., Ângelo, J., Andrade, L., Madeira, L.M., Mendes, A., 2013. An overview of photocatalysis phenomena applied to NOx abatement. J. Environ. Manag. 129, 522 539. https://doi.org/10.1016/j.jenvman.2013.08.006.

Arroyo, R., Córdoba, G., Padilla, J., Lara, V.H., 2002. Influence of manganese ions on the anatase-rutile phase transition of TiO2 prepared by sol-gel process. Mater. Lett. 54 (5 6), 397 402. https://doi.org/10.1016/S0167-577X(01)00600-0.

Baillon Martin, C., Michel, F., Vitrac, S., 2004. Regeneration process for chemical milling acids, installation for the implementation of the process and associated chemical milling method (Procédé de régénération des acides d'usinage chi- mique, installation pour la mise en œuvre du procédé et procédé d'usinage chimique associé). Patent FR2874220 France.

Bares, P., Cros, C., 2010. Method for regenerating a solution used for pickling or chemically milling titanium (Procédé de régénération d'une solution de décapage ou d'usinage chimique du titane). Patent WO2010139902A1 France.

Bloß, S.P., Elfenthal, L., 2007. Doped titanium dioxide as a photocatalyst for UV and visible light. In: Proceedings International RILEM Symposium on Photocatalysis, Environment and Construction Materials - TDP 2007, Florence, Italy, pp. 31 38.

Çakır, O., 2008. Chemical etching of aluminium. J. Mater. Process. Technol. 199 (1 3), 337 340. https://doi.org/10.1016/j.jmatprotec.2007.08.012.

Çakır, O., 2016. Chemical machining of CZ128 copper alloy. In: Conference on Ad- vances in Mechanical Engineering Istanbul - ICAME2016.

Çakır, O., Yardimeden, A., Ozben, T., 2007. Chemical machining. Arch. Mater. Sci. Eng. 28 (8), 499 502.

Cassar, L., 2004. Photocatalysis of cementitious materials: clean buildings and clean air. MRS Bull. 29 (5), 328 331. https://doi.org/10.1557/mrs2004.99.

Chen, Y.L., 1990. Chemical Milling of Titanium. U.S. Patent No 4900398. U.S. Patent and Trademark Office, Washington, DC.

Chrcanovic, B.R., Delany, M.M., 2014. Study of the influence of acid etching treat- ments on the superficial characteristics of Ti. Mater. Res. 17 (2), 373 380. https://doi.org/10.1590/S1516-14392014005000042.

El-Hofy, H.A.G., 2005. Advanced Machining Processes: Nontraditional and Hybrid Machining Processes. McGraw Hill Professional.

Fatima, R., Afridi, M.N., Kumar, V., Lee, J., Ali, I., Kim, K.H., Kim, J.O., 2019. Photo- catalytic degradation performance of various types of modified TiO2 against nitrophenols in aqueous systems. J. Clean. Prod. 231, 899 912. https://doi.org/ 10.1016/j.jclepro.2019.05.292.

Fisher, J., Edgerton, T.A., 2001. Titanium Compounds, Inorganic. Kirk-Othmer Encyclopedia of Chemical Technology. Wiley, New York.

Fujishima, A., Zhang, X., 2006. Titanium dioxide photocatalysis: present situation and future approaches. CR. Chim. 9 (5 6), 750 760. https://doi.org/10.1016/ j.crci.2005.02.055.

Gauvin, F., Caprai, V., Yu, Q.L., Brouwers, H.J.H., 2018. Effect of the morphology and pore structure of porous building materials on photocatalytic oxidation of air pollutants. Appl. Catal. B Environ. 227, 123 131. https://doi.org/10.1016/ j.apcatb.2018.01.029.

Gholami, A., Alemrajabi, A.A., Saboonchi, A., 2017. Experimental study of self-

cleaning property of titanium dioxide and nanospray coatings in solar applications. Sol. Energy 157, 559 565. https://doi.org/10.1016/j.solener.2017.08.075.
Guidance - Nitric Acid: Health Effects, Incident Management and Toxicology. Public Health England, Part of: Chemical Hazards Compendium, 12 January 2018. , Published: 1 July 2014. https://www.gov.uk/government/publications/nitric-acid-properties-incident-management-and-toxicology.
Guidance - Hydrogen Fluoride: Health Effects, Incident Management and Toxicology. Public Health England, Part of: Chemical Hazards Compendium, Published: 7 November 2017, 13 November 2017. https://www.gov.uk/government/publications/hydrogen-fluoride-health-effects-incident-management-and-toxicology.
Guimaraes, R.R., Parussulo, A.L., Araki, K., 2016. Impact of nanoparticles preparation method on the synergic effect in anatase/rutile mixtures. Electrochim. Acta 222, 1378 1386. https://doi.org/10.1016/j.electacta.2016.11.114.
Gusmerotti, N.M., Testa, F., Corsini, F., Pretner, G., Iraldo, F., 2019. Drivers and approaches to the circular economy in manufacturing firms. J. Clean. Prod. 230, 314 327. https://doi.org/10.1016/j.jclepro.2019.05.044.
Hanaor, D.A., Sorrell, C., 2011. Review of the anatase to rutile phase transformation. J. Mater. Sci. 46 (4), 855 874. https://doi.org/10.1007/s10853-010-5113-0.
Harris, W.T., 1976. Chemical Machining: the Technology of Cutting Materials by Etching. Clarendon Press.
Horgnies, M., Dubois-Brugger, I., Gartner, E.M., 2012. NOx de-pollution by hardened concrete and the influence of activated charcoal additions. Cement Concr. Res. 42 (10), 1348 1355. https://doi.org/10.1016/j.cemconres.2012.06.007.
Hot, J., Martinez, T., Wayser, B., Ringot, E., Bertron, A., 2016. Photocatalytic degradation of NO/NO2 gas injected into a 10-m3 experimental chamber. Environ. Sci. Pollut. Res. 1 9 https://doi.org/10.1007/s11356-016-7701-2.
Hot, J., Topalov, J., Ringot, E., Bertron, A., 2017. Investigation on parameters affecting the effectiveness of photocatalytic functional coatings to degrade NO: TiO2 amount on surface, illumination, and substrate roughness. Int. J. Photoenergy. https://doi.org/10.1155/2017/6241615.
Huang, Y., Ho, S., Lu, Y., Niu, R., Xu, L., Cao, J., Lee, S., 2016. Removal of indoor volatile organic compounds via photocatalytic oxidation: a short review and prospect. Molecules 21 (1), 56. https://doi.org/10.3390/molecules21010056.
Hüsken, G., Hunger, M., Brouwers, H.J.H., 2009. Experimental study of photocatalytic concrete products for air purification. Build. Environ. 44 (12), 2463 2474. https://doi.org/10.1016/j.buildenv.2009.04.010.
Jamieson, J.C., Olinger, B., 1969. Pressure-temperature studies of anatase, brookite rutile, and TiO2(II): a discussion. Am. Mineral.: J. Earth Planet. Mater. 54 (9 10), 1477 1481.
Kalinovskaya, I.V., Zadorozhnaya, A.N., 2016. Photolysis of light-transforming polymer materials on the basis of europium (III) nitrate with 1, 10-phenanthroline and anthranilic acid. Opt Spectrosc. 121 (3), 384 386. https://doi.org/10.1134/S0030400X16090083.
Kalinovskaya, I.V., Zadorozhnaya, A.N., Karasev, V.E., 2011. Photochemical behavior of lanthanide-containing polymer materials. Russ. J. Gen. Chem. 81 (5), 819 823. https://doi.org/10.1134/S1070363211050045.
Lasek, J., Yu, Y.H., Wu, J.C., 2013. Removal of NOx by photocatalytic processes. J. Photoch. Photobio. C. 14, 29 52. https://doi.org/10.1016/j.jphotochemrev.2012.08.002.
Laufs, S., Burgeth, G., Duttlinger, W., Kurtenbach, R., Maban, M., Thomas, C., Wiesen, P., Kleffmann, J., 2010. Conversion of nitrogen oxides on commercial photocatalytic dispersion paints. Atmos. Environ. 44 (19), 2341 2349. https://doi.org/10.1016/j.atmosenv.2010.03.038.
Liu, G., Yan, X., Chen, Z., Wang, X., Wang, L., Lu, G.Q., Cheng, H.M., 2009. Synthesis of rutile-anatase core-shell structured TiO2 for photocatalysis. J. Mater. Chem. 19 (36), 6590 6596. https://doi.org/10.1039/B902666E.
Lorencik, S., Yu, Q.L., Brouwers, H.J.H., 2015. Design and performance evaluation of the functional coating for air purification under indoor conditions. Appl. Catal. B Environ. 168, 77 86. https://doi.org/10.1016/j.apcatb.2014.12.012.
Markle, R., 2015a. Etching Titanium with HF and Nitric Acid Solutions Part 1. Chemcut Corporation. http://www.chemcut.net/wp-content/uploads/2015/02/Etching-Titanium-with-HF-and-Nitric-Acid-Solutions-Part1.pdf. accessed April 2017.
Markle, R., 2015b. Etching Titanium with HF and Nitric Acid Solutions Part 2. Chemcut Corporation. http://www.chemcut.net/wp-content/uploads/2015/02/Etching-Titanium-with-HF-and-Nitric-Acid-Solutions-Part2.pdf. accessed April 2017.
Marsuhashi, R., Takahashi, K., 2002. The integral rate equation of pure titanium in nitric-hydrofluoric acid solutions. Nippon steel technical report. Overseas 85, 59 63. http://www.nssmc.com/en/tech/report/nsc/pdf/8512.pdf. accessed March 2017.
Martinez, T., 2012. Photocatalytic coatings for construction materials: Formulation, efficiency assessment and ecotoxicity (Revêtements photocatalytiques pour matériaux de construction: Formulation, évaluation de l'efficacité et écotoxicité). PhD thesis. Université Toulouse III-Paul Sabatier.
Martinez, T., Bertron, A., Ringot, E., Escadeillas, G., 2011. Degradation of NO using photocatalytic coatings applied to different substrates. Build. Environ. 46 (9), 1808 1816. https://doi.org/10.1016/j.buildenv.2011.03.001.
Martinez, T., Bertron, A., Escadeillas, G., Ringot, E., Simon, V., 2014. BTEX abatement by photocatalytic TiO2-bearing coatings applied to cement mortars. Build. Environ. 71, 186 192. https://doi.org/10.1016/j.buildenv.2013.10.004.
McGee, J.J., Heicklen, J., 1964. Photolysis of nitric oxide. J. Chem. Phys. 41 (10), 2974 2977.
Meyer, S., Gorges, R., Kreisel, G., 2004. Preparation and characterization of titanium dioxide films for catalytic applications generated by anodic spark deposition. Thin Solid Films 450 (2), 276 281. https://doi.org/10.1016/j.tsf.2003.11.168.
Mills, A., Elliott, N., Parkin, I.P., O'Neill, S.A., Clark, R.J., 2002. Novel TiO2 CVD films for semiconductor photocatalysis. J. Photochem. Photobiol., A 151 (1 3), 171 179. https://doi.org/10.1016/S1010-6030(02)00190-9.
Nicolas, M., 2018. Procédé de régénération d'un bain d'usinage chimique de pièces en titane. Castelginest, FRANCE Brevet Patent Application WO/2018/229672.
Ohno, T., Sarukawa, K., Matsumura, M., 2002. Crystal faces of rutile and anatase TiO2 particles and their roles in photocatalytic reactions. New J. Chem. 26 (9), 1167 1170. https://doi.org/10.1039/B202140D.
Pozo-Antonio, J.S., Dionísio, A., 2017. Self-cleaning property of mortars with TiO2 addition using real diesel exhaust soot. J. Clean. Prod. 161, 850 859. https://doi.org/10.1016/j.jclepro.2017.05.202.
Rambabu, Y., Jaiswal, M., Roy, S.C., 2016. Effect of annealing temperature on the phase transition, structural stability and photo-electrochemical performance of TiO2 multi-leg nanotubes. Catal. Today 278, 255 261. https://doi.org/10.1016/j.cattod.2016.01.016.
Ren, H., Koshy, P., Chen, W.F., Qi, S., Sorrell, C.C., 2017. Photocatalytic materials and technologies for air purification. J. Hazard Mater. 325, 340 366. https://doi.org/10.1016/j.jhazmat.2016.08.072.
Sanz, M.C., 1956. Process of Chemically Milling Structural Shapes and Resultant Article. USA Patent No: 2739047.
Schneiker, T., Forsberg, K., 2014. Process chemistry and acid management for titanium pickling processes. In: Conference on Titanium Europe, Sorrento, pp. 19 21.
Serna, F., Lagneau, J., Carpentier, J.M., 2014. X-ray diffraction: a powerful technique to solve some industrial and technological problems (La diffraction des rayons X: une technique puissante pour résoudre certains problemes industriels et technologiques). Chem. Nouv. 11, 1 12. http://chimienouvelle.be/CN116web/CN166%20serna.pdf. accessed January 2017.
Shannon, R., Pask, J.A., 1965. Kinetics of the anatase-rutile transformation. J. Am. Ceram. Soc. 48 (8), 391 398.
Silva, C.G., Wang, W., Faria, J.L., 2006. Photocatalytic and photochemical degradation of mono-, di- and tri-azo dyes in aqueous solution under UV irradiation. J. Photochem. Photobiol., A 181 (2 3), 314 324. https://doi.org/10.1016/j.jphotochem.2005.12.013.
Spurr, R.A., Myers, H., 1957. Quantitative analysis of anatase-rutile mixtures with an X-ray diffractometer. Anal. Chem. 29 (5), 760 762.
Suárez-Eiroa, B., Fernández, E., Méndez-Martínez, G., Soto-Onate, D., 2019. Operational principles of circular economy for sustainable development: linking theory and practice. J. Clean. Prod. 214, 952 961. https://doi.org/10.1016/j.jclepro.2018.12.271.
Sutter, E.M.M., Goetz-Grandmont, G.J., 1990. The behaviour of titanium in nitric-hydrofluoric acid solutions. Corros. Sci. 30 (4 5), 461 476. https://doi.org/10.1016/0010-938X(90)90051-6.
Taguchi, T., Saito, Y., Sarukawa, K., Ohno, T., Matsumura, M., 2003. Formation of new crystal faces on TiO2 particles by treatment with aqueous HF solution or hot sulfuric acid. New J. Chem. 27 (9), 1304 1306. https://doi.org/10.1039/B304518H.
Tal-Gutelmacher, E., Eliezer, D., 2004. Hydrogen-assisted degradation of titanium based alloys. Mater. Trans. 45 (5), 1594 1600. https://doi.org/10.2320/matertrans.45.1594.
Tehrani, A.F., Imanian, E., 2004. A new etchant for the chemical machining of St304. J. Mater. Process. Technol. 149 (1 3), 404 408. https://doi.org/10.1016/j.jmatprotec.2004.02.055.
Topalov, J., Hot, J., Ringot, E., Bertron, A., 2019. In situ NO abatement by photocatalysis study under continuous NO injection in a 10-m3 experimental chamber. Air Qual. Atmos. Health 12 (2), 229 240. https://doi.org/10.1007/s11869-018-0644-7.
Verdier, T., Coutand, M., Bertron, A., Roques, C., 2014. Antibacterial activity of TiO2 photocatalyst alone or in coatings on E. coli: the influence of methodological aspects. Coatings 4 (3), 670 686. https://doi.org/10.3390/coatings4030670.
Yamamoto, K., Lim, E., Ito, K., 2014. Performance evaluation of reduction in VOC concentration by photocatalytic building materials in a real-scale chamber. In: Indoor Air 2014 - 13th International Conference on Indoor Air Quality and Climate.
Zhang, W., Tang, H., 2018. Rutile nanopowders for pigment production: formation mechanism and particle size prediction. Chem. Phys. Lett. 692, 129 133. https://doi.org/10.1016/j.cplett.2017.12.025.